Spectroscopic study of gap-surface plasmons in a metallic convex groove array and their applications in nanofocusing and plasmonic sensing

Daimin Li,[1,*] Jun-Yu Ou,[2,*] Peng Xie,[1] Zhengchen Liang,[3] Wei Wang,[3,†] Wenxin Wang,[4,5] Hong Zhang,[3,6] and Xiaoyu Kuang[1]

[1]*Institute of Atomic and Molecular Physics, College of Physics, Sichuan University, Chengdu 610065, China*
[2]*Optoelectronics Research Centre and Centre for Photonic Metamaterials, University of Southampton, Highfield, Southampton SO17 1BJ, United Kingdom*
[3]*College of Physics, Sichuan University, Chengdu 610064, China*
[4]*College of Physics and Optoelectronic Engineering, Harbin Engineering University, 150001 Harbin, China*
[5]*Qingdao Innovation and Development Base, Harbin Engineering University, Qingdao 266500, China*
[6]*Key Laboratory of High Energy Density Physics and Technology of Ministry of Education, Sichuan University, Chengdu 610065, China*

(Received 20 October 2020; revised 16 May 2021; accepted 18 May 2021; published 2 June 2021)

Plasmonic tapered grooves have been proven to be good candidates for the excitation of gap surface plasmons (GSPs), surface plasmons trapped vertically inside a metallic tapered groove or slit. GSPs have attracted tremendous interest due to their unique properties of concentrating light in nanosized gaps with significant field enhancement, thus offering potential applications such as ultracompact nanocircuits, broadband light absorbers, and plasmonic sensors. In this paper, we focus on GSPs supported by periodic arrays of narrow convex grooves and study in detail their properties by using visible-near-infrared (VIS-NIR) spectroscopy. We identify strong second- and third-order GSP modes excited in ultrasharp convex grooves. The dependence of GSP resonances on the groove profile is analyzed with the help of detailed full-wave simulations, revealing the fact that an ultrasharp, but finite, gap exists at the groove bottom and plays a crucial role in determining both the GSP resonance positions and the nanofocusing capability with much improved field enhancement inside the grooves. Spectral shifts of the observed GSP resonances relative to the simulation results are found in a shorter wavelength range and are qualitatively explained as nonlocal effects originating from the nonclassical microscopic behavior of local currents and charges at imperfect interfaces. Utilizing such strong and distinguishable GSP resonance line shapes in an otherwise flat reflectivity spectral baseline, we experimentally demonstrate the capability of convex groove arrays to perform dual-band refractive index sensing in the VIS-NIR range.

DOI: 10.1103/PhysRevB.103.245404

I. INTRODUCTION

With the ability to control light at the nanoscale by excitation of surface plasmon polaritons (SPPs), metallic nanostructures play a crucial role in various applications [1]. Tapered nanostructures consisting of grooves with different shapes on a planar metal film or surface have attracted tremendous interest due to their capability of supporting gap-surface plasmon (GSP) modes, that is, propagating SPPs between two close metal interfaces separated by a dielectric gap [2–5]. GSP excited in tapered grooves exhibits advantageous properties over the usual propagating SPP mode due to its nanofocusing ability to guide and concentrate electromagnetic field [6], leading to nanoscale confinement [7,8], boosted extraordinary optical transmission (EOT) [9], and highly efficient light absorption [10,11]. These distinctive GSP features may help design advanced functional devices such as ultracompact photonic components, efficient broadband light absorbers, and enhanced extraordinary optical transmission filters (see the review article in [12] and references therein).

GSP characteristics have been intensively studied in a variety of nanostructures. Theoretical and experimental studies have convincingly revealed the nanofocusing effect of GSP for the local field enhancement (FE) in one-dimensional (1D) gratings of plasmonic V-shaped grooves [13–15]. Detailed investigations have been focused on interacting V grooves in two-dimensional (2D) periodic arrays, aiming to achieve higher FE with the help of GSP nanofocusing at the tapered bottom of the V groove [16]. Arrays of V-shaped slits have also been studied for their promising application in extraordinary optical transmission due to the GSP nanofocusing effect resulting from the tapered slits [9,17,18].

In addition to the aforementioned 1D/2D V-shaped plasmonic array with large, flat groove/slit separations, tapered grooves with convex sidewalls curving toward the bottom of the groove and ending with ultrasharp groove tips have drawn much attention due to the unique GSP propagating property inside the grooves and, particularly, at their bottom, which leads to a much larger FE and nanofocusing effect. Detailed investigations of the optical response of a 1D/2D ultrasharp

*These authors contributed equally to this work.
†w.wang@scu.edu.cn

convex groove array with no flat surfaces have demonstrated the capability of realizing "plasmonic black metals" with broadband nonresonant light absorption via adiabatic nanofocusing of GSP modes traveling down to the groove tips [14]. It has been shown that both the GSP propagation and the nonresonant light absorption are dependent on the groove geometry, including the groove depth, the width at the trench opening, the sidewalls, and the angle of the bottom of the groove.

In contrast to these groove arrays with a vanishing flat section between groove separations exhibiting the nonresonant nanofocusing effect, tapered groove/slit arrays with a large, flat section generally support highly distinguishable resonant GSPs, which are beneficial for the resonant nanofocusing effects, enhanced EOT, and plasmonic sensing. Although theoretical and experimental works have been conducted well to explore the GSP property [9,14,19], only a few studies focused on the optical response of the convex groove array with an ultrasharp profile at the bottom of the groove. Detailed spectroscopic characterization and, particularly, the analytical dependence of the spectral response on the gap width at the bottom of the groove have not been reported.

In this paper, using visible-near-infrared (VIS-NIR) spectroscopy, we study in detail the optical response of 1D convex groove arrays with large, flat separations and ultrasmall width at the groove bottom. We identify strong second- and third-order GSP modes excited by ultrasharp convex grooves. With the full-wave simulations, the dependence of GSP resonances on the groove profile is analyzed in detail. We reveal that the ultrasharp finite gap exists at the bottom of the groove and plays a crucial role in determining both the GSP resonance positions and the nanofocusing capability with improved field enhancement inside the grooves. We analyze the spectral shifts of the observed GSP resonances relative to the simulation results, which is qualitatively explained as nonlocal effects originating from the nonclassical microscopic behavior of local currents and charges at imperfect interfaces. Furthermore, we experimentally demonstrate a dual-band refractive index sensor in the VIS-NIR range using a convex groove array which exhibits strong and salient GSP resonances.

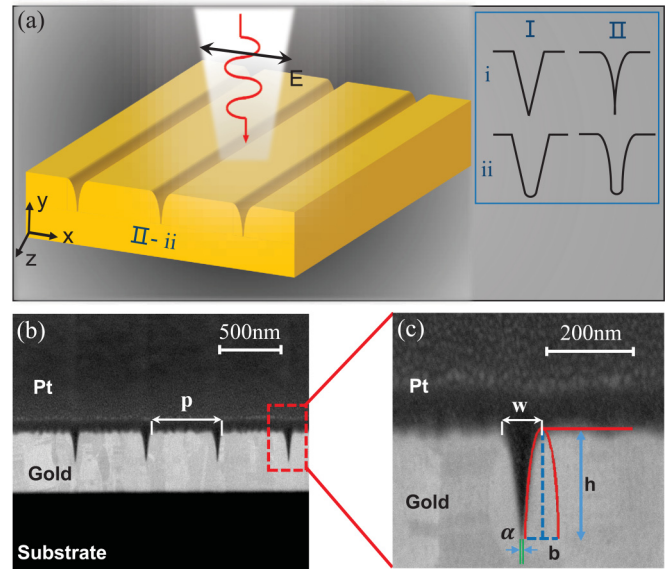

FIG. 1. (a) Three-dimensional schematic illustration of the metallic convex groove array. Four types of groove profiles are given in the inset: linear (I) and convex-shaped (II) taper with zero-width bottom (i) and round apex (ii). (b) Scanning electron micrograph of a 1D array of metallic convex grooves (scale bar is 500 nm) with a period of p. (c) Zoom-in image of one groove with groove depth h, trench width w, and bottom width α. The half ellipse (red curve) with semimajor axis h and semiminor axis b marks the groove profile.

II. RESULTS AND DISCUSSION

A. Convex groove array: Fabrication and characterization

The 1D groove array studied here, as depicted in Fig. 1(a), features convex-shaped tapers with a round apex (type II-ii in the inset), which is different from the convex groove array containing tapers with a zero-width bottom (type II-i) and their linear counterparts (types I-i and I-ii). The influence of the convex sidewall and round apex (ultrasharp groove tips with a finite width) on the optical response of the patterned array will be discussed in a later Sec. II A. The convex groove arrays were fabricated by focused-ion-beam (FIB; Helios Nanolab 600, FEI Company) milling on a surface of a thin gold film. First, a gold film (500 nm thick) was deposited on a quartz substrate by a magnetron sputtering system (DE500, TE technology). A thin layer of Cr film (∼3 nm thick) was deposited on the substrate before the deposition of the Au film for better adhesion. The groove arrays were then prepared on the Au film by FIB milling at 30 kV acceleration voltage and a beam current of 10 pA. By applying an optimized dwell time, we obtained the desired groove patterns with high precision by just varying the number of passes. The experimental spectra were obtained using a microspectrophotometer (CRAIC QDI2010), with a $20 \times 20\,\mu m^2$ collection aperture via a $15\times$ objective with a numerical aperture of 0.28.

Figure 1(b) gives a side-view scanning electron micrograph (SEM) image of the fabricated groove array, illustrating a clear convex groove profile, which exhibits convex sidewalls, rounding curvatures at the trench openings, and ultrasharp groove tips with a finite width. The groove profile, key for determining the optical response of the patterned array, can be characterized by the following main structural parameters: the period p, the sidewall of groove described by a $1/4$ ellipse with a semimajor axis h and a semiminor axis b, the width w, and the gap width characterized by a half circle with a diameter α, as depicted in Fig. 1(c). Note that the fabricated grooves exhibit apparent asymmetrical sidewalls. The influence of the asymmetry of the sidewalls on the GSP property will be discussed in detail later.

We systematically investigate the GSP excitation and the resulting optical properties of such a 1D groove array by manufacturing two sets of samples with different groove depths and trench widths. We first focus on the first sample (labeled 1) with period $p = 600$ nm, groove depth $h \approx 180$ nm, and trench width at the top of about $w \approx 60$ nm estimated from the cross section of the SEM image, as shown in Fig. 1(c). For such a convex groove array, we measured the reflectance spectrum under the illumination of a linearly polarized light at normal incidence with its magnetic component along the groove. The measured reflectance spectrum

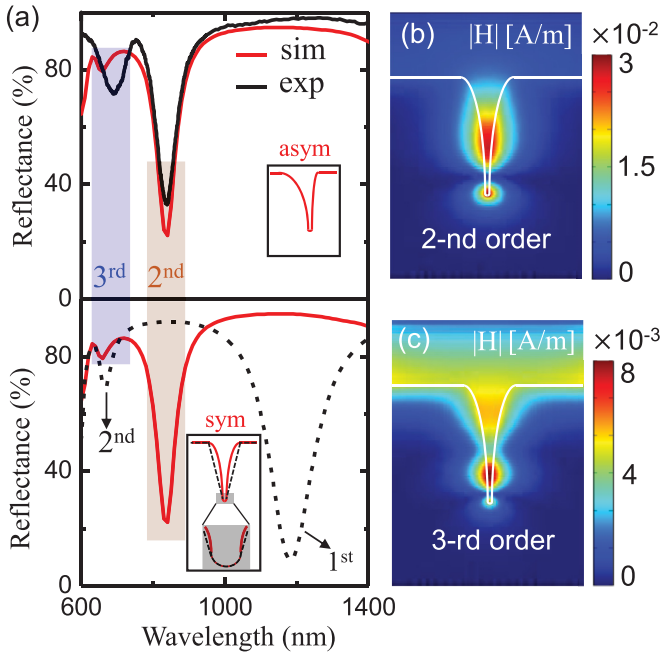

FIG. 2. (a) Top: measured (black) and simulated (red) reflectance spectra at normal incidence for asymmetrical metallic groove array of sample 1 in air. Bottom: simulated reflectance spectra for symmetrical (solid line) and tapered (dashed line) metallic groove array in air. The inset shows the geometrical details of the groove tip. Magnetic field in color scale (b) at second-order GSP resonance $\lambda_{GSP} = 840$ nm and (c) at third-order GSP resonance $\lambda_{GSP} = 660$ nm. The white lines mark the gold-dielectric interface.

(solid black line), as shown in the top panel of Fig. 2(a), exhibits two distinct dips, corresponding to the excitation of the second-order GSP at $\lambda_{GSP2} = 839$ nm (yellow shade) and the third-order GSP at $\lambda_{GSP3} = 688$ nm (blue shade), respectively.

To verify the GSP excitations, we further conducted numerical simulations by using the finite-difference time-domain method. Here, the permittivity of bulk gold in the VIS-NIR range is described by Ref. [20]. It should be emphasized that (i) the fine details of the groove profile such as the gap width at the groove bottom are not visible at the SEM scale and (ii) our simulation indicates that the GSP response is mainly dependent on the shape of the groove sidewalls, the groove depth, the trench width, and, particularly, the width at the groove bottom. Therefore, in our simulation, the groove profile was built according to the parameters observed from the SEM image to match the practical groove shape. Then we carefully performed the simulation with a variety of structural parameters with fine tuning of the gap width at the groove bottom to reproduce the experimental observation. We can successfully reproduce the measured reflectance spectrum with reasonably good matching, as displayed in the top panel of Fig. 2(a) (solid red line) with the optimized geometry of groove width $w = 58$ nm; an ellipse with a semimajor axis $h = 176$ nm, semiminor axis $b = 27.9$ nm, and bottom width $\alpha = 2.2$ nm; and the grid used for simulation being 0.2 nm.

In reality, the fabrication process generates asymmetrical sidewalls, as clearly shown in Fig. 1(b). To demonstrate the influence of the asymmetry of the sidewalls on the GSP excitations, we also compared with a groove structure with symmetric sidewall keeping other structural parameters fixed. The simulated spectrum as given in the bottom panel of Fig. 2(a) (solid red line) shows features similar to the asymmetrical case, which indicates that the asymmetry of the groove shape has a negligible effect on the GSP excitations. From this point, we stick to the symmetrical configuration in our following simulations of the fabricated samples for the simplification of the model and the analysis. The GSP excitations can clearly be identified by the simulated near-field response at the resonance wavelengths [21]. Figures 2(b) and 2(c) give the magnetic field distribution at GSP resonance wavelengths of 840 and 660 nm, exhibiting, respectively, two and three lobes in the standing wave pattern. This evidences that the measured excited GSP modes are, indeed, the second- and third-order GSP modes, respectively.

To demonstrate the influence of the sidewall profile on the GSP property, we also analyzed the optical response of linear tapers while keeping the other parameters used for the convex groove, as shown in the inset of Fig. 2(a) (dashed black profile). In this case, the groove array exhibits a distinctly different reflectance spectrum with GSP resonances that are dramatically blueshifted (dashed black profile). The near-field analysis confirms the first-order GSP mode around 1.2 μm in the NIR range and the second-order mode around 700 nm in the visible range, which overlaps the third-order GSP resonance in the convex groove, showing the significant impact of the sidewall curvature. In our simulation obvious of Fig. 2(a), the groove profile was carefully built based on the SEM image in such a way that the experimental results can be well reproduced.

B. Dependence of GSP resonances on the width at the groove tip

As mentioned in the previous section, in addition to from the groove depth, the trench width, and the curvature of the sidewall, the bottom width of the groove may also exert significant influence on the GSP excitations and the resultant optical property of the groove array. The structural effects on the optical response have been observed in 1D convex grooves for broadband nonresonant total absorption [10]. However, a detailed analysis of the relevance of the width of the bottom for the GSP resonance has not been performed. Here, we study the relationship between the GSP resonances and the width of the bottom of the groove by combining the measured spectral response with detailed simulations. We will prove the fact that the ultrasharp profile exists at the bottom of the groove and plays a crucial role in both the GSP resonance positions and the nanofocusing capability with the field enhancement inside the grooves.

We first performed simulations to evaluate the general dependence of the GSP resonance on the width of the bottom α. For sample 1, we slightly increase the width of the bottom from its optimized value to 4 nm with other parameters fixed, and surprisingly, the second-order GSP resonance dramatically shifts by over 50 nm to the blue, as clearly shown in Fig. 3(a). It should be emphasized that the spectrum for the zero-width bottom (blue), i.e., touching sidewalls at an apex with $\alpha = 0$ nm, shows distinctly different aspects: it exhibits a flat reflection curve without salient GSP resonances. This

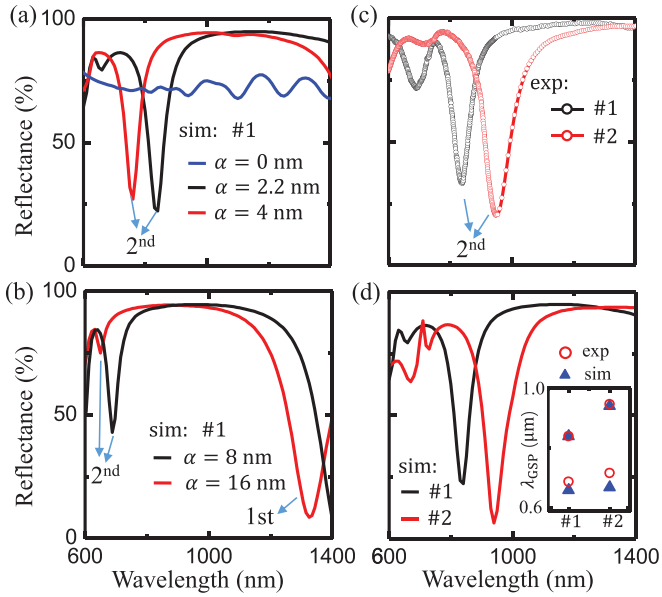

FIG. 3. (a) and (b) Simulated reflectance spectra for sample 1 at normal incidence with parameters $p = 600$ nm, $w = 58$ nm, $h = 176$ nm, and $b = 27.9$ nm. (c) The measured reflectance spectra of sample 1 (black) and sample 2 (red) and (d) the corresponding simulated reflectance spectra of sample 1 (black) and sample 2 (red) with $\alpha = 2.4$ nm. The inset gives the resonance wavelengths of the two samples obtained from the experiments (circles) and simulations (triangles).

effect has also been observed in other studies on 1D plasmonic grooves [22,23]. We also performed the simulation for the groove array with bottom width $\alpha = 8$ nm, nearly four times larger than the optimized value $\alpha = 2.2$ nm. Such a large bottom width causes an apparent change in the reflectance spectrum with a significant blueshift of the first-order GSP resonance by ~300 nm, as shown in Fig. 3(b) (black line). In this case, if we change (increase or decrease) the width of the bottom by nearly the same absolute amount (8 nm), the spectrum (red line) is not strongly altered. The above simulation results clearly indicate two facts: (i) the GSP resonances are very sensitive to a small change in the width of the bottom in the case of a narrow gap (several nanometers), and (ii) a finite gap does exist at the bottom of the fabricated grooves, exactly in the range of a few nanometers, although this tiny gap size can hardly be distinguished in the SEM image. The above simulations show that the measured spectrum can be reproduced only if the finite bottom width is precisely set to a few nanometers, as shown in our case.

To confirm this structural dependence, we further designed and fabricated the other groove array (labeled sample 2, $p = 600$ nm) with larger groove depth $h = 240$ nm and trench width $w = 80$ nm. The measured reflectance spectrum (red circles), as shown in Fig. 3(c), shows the first- and second-order GSP resonances that are considerably shifted to red. This spectrum can be readily reproduced in our simulation with the optimized groove parameters $p = 600$ nm, $h = 238$ nm, $b = 43.8$ nm, $w = 90$ nm, and $\alpha = 2.4$ nm, as demonstrated in Fig. 3(d) (red line).

It is worth noting that discrepancy between the simulation and experiment is found in the spectral response of GSP modes, particularly for the second-order GSP mode in the shorter wavelength (higher frequencies) range, as shown in the inset of Fig. 3(d). A similar discrepancy has also been reported in plasmonic film-coupled nanoresonators [24], which was explained as nonlocal effects originating from the nonclassical microscopic behavior of local currents and charges at imperfect interfaces. Such nonlocal effects have been included in a nonclassical model by introducing highly dispersive surface-response functions known as Feibelman d parameters at the material interface [25], which can be translated directly into observable-spectral shifts and broadening with the help of quasinormal-mode perturbation theory [26,27]. In our case as well, the spectral shifts can be attributed to nonlocal effects since our experiments (optical response obtained by reflectance measurements) and careful simulations provide convincing evidence for the existence of the ultrasharp gap at the bottom of the groove (on the scale of a few nanometers). Here, we give a qualitative analysis of such effects. The nanosized gap at the groove bottom is very much analogous to that in the multistacked planar metal-dielectric-metal nanostructure, where localized gap-plasmon resonances exhibit prominent spectral shifts concerning the classical predictions due to the strong nonclassical perturbation strength at the interfaces of the gold film-nanodisk gap [24]. Although the thickness of the dielectric spacer (AlO_x) is comparable to the gap width of the groove in our case, the spectral shifts reported here are less prominent. This can be explained by the following two facts: (i) Much stronger field confinement can be achieved beneath the entire nanodisk footprint in the film-coupled gaps. This is in contrast to the groove with a limited gap region, leading to weaker field enhancement with reduced perturbation strength. (ii) The air-metal interface of the present groove gap favors the injection of induced charges into the gold sidewalls, thus reducing the nonlocal effects relative to the dielectric-metal interface with considerable screening effects from the dielectric material with high refractive index.

It was also reported that another quantum phenomenon called electron spill-out effects may also occur in ultrasharp metallic gaps [28]. For a gap of subnanometer size, a distance comparable to the length scale of the electron spill out from the metallic interfaces, the conduction electrons can tunnel through the potential barrier across the junction and start to overlap, thus greatly modifying the local electron densities at the metal surfaces and leading to distinctly different plasmonic response with respect to classical predictions. Since the conduction electron density profile generally extends within the range of ~0.2 nm outside the surface [29], the spill-out effect generally starts to dominate for the case of gap width less than 1 or even 0.5 nm. Therefore, we do not consider such effects in our case.

It is also noted that the excitation of GSP modes for both samples leads to dips in the reflectance spectra with large amplitudes. The formation of the resonance peaks is related to the propagation of GSP modes inside the grooves, which bears resemblance to the occurrence of GSP resonances in V-shaped grooves/slits [9,15], but the output reflection spectra for these two cases are distinctly different, as shown in Fig. 3(a). In the case of V grooves, the GSP electric field drastically and

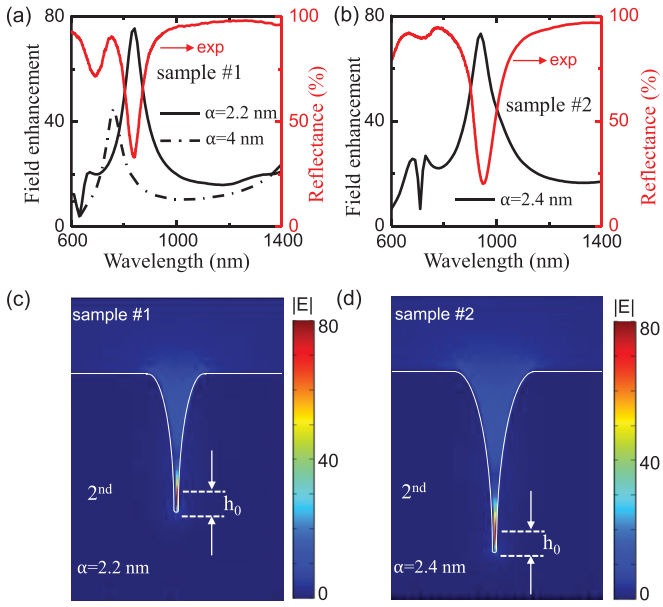

FIG. 4. (a) and (b) Field enhancement (black curve) calculated at the groove bottom as a function of wavelength for sample 1 and sample 2 with $\alpha = 2.2$ nm (black dash-dotted line), respectively. The corresponding measured reflectance spectra are given by red curves. (c) and (d) Calculated normalized field magnitude distributions for sample 1 at $\lambda_{GSP} = 840$ nm and sample 2 with $\lambda_{GSP} = 940$ nm.

rapidly decreases as it reaches the groove bottom, causing two counterpropagating GSP waves that are almost out of phase with a reflection phase φ_r close to π [15]. Their destructive interference accounts for the reflection spectra with low contrast. However, in the present convex grooves, well-separated GSP modes with much deeper reflection dips are observed, which indicates significant field enhancement inside the grooves due to the strong nanofocusing effect. Such a strong GSP response is beneficial for finding potential use in a variety of applications. In the following sections, we will discuss in detail the GSP suitability for nanofocusing and sensing applications.

C. Nanofocusing capability: Field enhancement

Radiation nanofocusing, featured by the concentration of electromagnetic fields beyond the diffraction limit, is an important research area in nano-optics and plasmonics with a variety of promising applications where drastic enhancement of localized optical field is required [9,15,30]. Here, we analyze the resonant nanofocusing effect using numerical simulations of the near-field response and the measured far-field spectral property of the convex groove array. In our simulations, a *p*-polarized wave is used to illuminate the grooves at normal incidence, with its magnetic field oscillating along the groove axis. Generally, a strong field enhancement occurs at the bottom of the groove, with the frequency-dependent location of the field maximum shifting towards the groove trench for longer wavelengths (lower frequencies) [15]. Therefore, a trade-off position of $h_0 = 18$ nm above the bottom of the groove was used in our simulation to monitor the nanofocusing effect for both samples. Figures 4(a) and 4(b) give the simulated field enhancement factor (black curves) as a function of wavelengths for sample 1 and sample 2, respectively. Several aspects can be seen: (i) pronounced field enhancement occurs at the second-order GSP resonances with a maximum enhancement factor up to 80, (ii) around the third-order GSP resonances [$\sim$630 nm in Fig. 4(a) and $\sim$700 nm in Fig. 4(b)], the field enhancement spectra show apparent dips instead of peaks, and importantly, (iii) the field enhancement is very sensitive to the width of the groove bottom α. As the width of the bottom increases to $\alpha = 4$ nm for sample 1, the field enhancement peak, as plotted in Fig. 4(a) (dash-dotted line), shifts following the GSP resonances shown in Fig. 3(a), which confirms the manifestation of resonant GSP nanofocusing in the present groove arrays.

For the tapered grooves reported in Ref. [9], the field enhancement factor reaches about 20 for both shallow (several hundreds of nanometers) and deep (several micrometers) grooves caused by the interference between the counterpropagating GSP waves reflected at the groove bottom and the trench opening. In this sense, the present convex groove array with pronounced GSP response is more favorable in concentrating light at the nanoscale since much higher field enhancement over 80 can be obtained at GSP resonances with much shallower grooves.

The nanofocusing effects can be better visualized by looking into the near-field response around the groove. Figures 4(c) and 4(d) provide the simulated normalized magnitudes of the electric field distribution at the second-order GSP resonances for samples 1 and 2, respectively. The magnitude distribution of the electric field inside the groove exhibits the standing-wave feature with the magnitude maximum located around h_0. Interestingly, the electric field is mainly localized at the small gap formed by the two nearly parallel sidewalls, which is in contrast to the V-groove case with maximum field confinement exactly at the groove bottom. It is noted that a reduction of the enhancement factor happens at the third-order GSP resonance around 700 nm [black curve in Fig. 4(b)]. This is mainly due, however, to the fact that the field maximum at the third-order GSP frequency dramatically shifts away from the monitored position h_0.

D. Dual-band refractive index sensing

In this section, we discuss the suitability of the convex groove array in the plasmonic sensing application at very small volumes. Here, we demonstrate the performance of the device and the potential application of the groove arrays as refractive index sensors. A small change in refractive index is recorded as the GSP resonance shift in the reflectance spectrum. Our approach is to use a calibrated refractive index oil on the groove surface to provide a small change in the refractive index around the groove. Now, we discuss the sensing characteristics of the two samples. In Fig. 5(a), we plot the measured reflectance spectrum as a function of different refractive indices for sample 1. Using the same geometric parameters as in the previous sections, we further obtain the simulated reflectance spectra [Fig. 5(b)], which are in good agreement with the experimental results. It is noted in the experimental reflectance spectra in Fig. 5(a) that pronounced dips (around 900 nm) are observed between the second- and

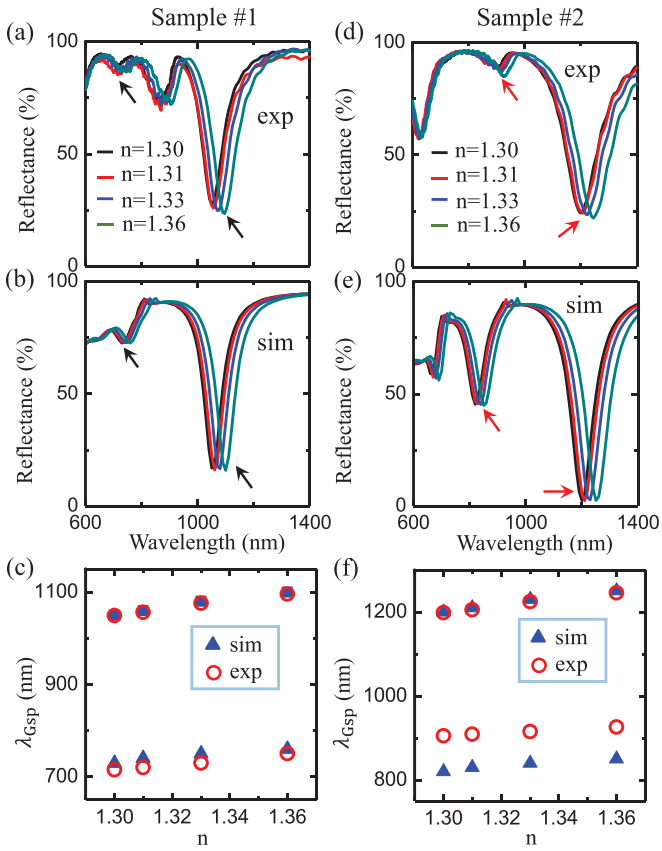

FIG. 5. (a) and (d) Measured and (b) and (e) simulated reflectance spectra of (a) and (b) sample 1 and (d) and (e) sample 2 with different refractive indices. (c) and (f) The GSP resonance positions as a function of refractive indices for (c) sample 1 and (f) sample 2 obtained from the experiments (circles) and simulations (triangles).

third-order GSP resonances for all refractive indices. These dips also appear at the same wavelengths in the simulated reflection spectra, but with much weaker amplitudes, as clearly shown in Fig. 5(b). This can also be explained as the consequence of the nonlocal effect. These spectral dips are found not in either the measured or simulated spectra for the two bare groove samples [Fig. 2(a)], indicating that the nonlocal perturbation strength is smaller to that in the groove arrays covered by dielectrics due to the reduction of the screening effect at the air-metal interface. This is consistent with the observations in the film-coupled nanoresonators reported in Ref. [24].

To quantitatively describe the performance of the present groove arrays as sensing devices, we focus on the second- and third-order of GSP resonances to demonstrate the possibility of the convex groove array in realizing dual-band refractive index sensing in the VIS-NIR range. In the measured reflectance spectrum of sample 1, we extracted the second- and third-order wavelength positions (black arrows) of the GSP resonance (λ_{GSP2} and λ_{GSP3}) with different refractive indices n_d, as shown by the red circles in Fig. 5(c). The measured second- and third-order GSP resonance shifts are linearly dependent on refractive indices of the atop medium, which is confirmed by the simulation results (blue triangles).

To evaluate the sensitivity, consider that the shift of GSP resonance peaks is proportional to the change in the linear refractive index; the first derivative of the GSP wavelength λ_{GSP} vs the refractive index n_d is approximately equivalent to a certain amount of GSP resonance shift in the corresponding refractive index change. The sensor sensitivity is calculated in the following form:

$$S = \frac{d(\lambda_{GSP})}{d(n_d)} \approx \frac{\Delta(\lambda_{GSP})}{\Delta(n_d)}. \quad (1)$$

Here, for sample 1, we calculated the refractive index change $\Delta(n_d) = 1.36 - 1.30 = 0.06$, which corresponds to the second- and third-order of GSP resonance shifts $\Delta(\lambda_{GSP2}) = 47$ nm from 1049 to 1096 nm and $\Delta(\lambda_{GSP3}) = 35$ nm from 715 to 750 nm, respectively. In this sense, we can readily calculate the corresponding sensitivities as 783 and 583 nm/RIU (RIU: refractive index unit), respectively. Using the same method, we also analyzed the sensor performance of sample 2. Figures 5(d) and 5(e) give the experimental and simulated reflectance spectra with different refractive indices n_d. The second- and third-order GSP resonance shifts (red arrows) with different refractive indices n_d were then extracted from these two sets of spectra and are compared with the values obtained from simulations in Fig. 5(f). Here, the sensitivity of the second- and third-order GSP resonances of the sample are 833 and 500 nm/RIU, respectively. This high-performance dual-band sensing capability originates from strong and distinguishable GSP resonances, which are sensitive to both the groove profile and the surrounding materials. One can carefully design a groove configuration such that the GSP resonances can be readily tuned to the desired wavelengths to realize dual-band sensing in the visible to NIR range. The working wavelength for sensing can be shifted to red over 100 nm with sensitivity similar to an array of deeper grooves, as clearly shown in Figs. 5(c) and 5(f). This constancy in the sensitivity is expected to hold for even deeper grooves.

III. CONCLUSIONS

In conclusion, we have experimentally demonstrated GSP properties of a simple 1D metallic convex groove array with large, flat separations and, above all, ultrasmall width at the bottom of the groove. By discussing the influence of structural parameters on GSP resonances, we have demonstrated the formation of GSP resonances of different orders. We revealed that an ultrasharp finite gap exists at the groove bottom and plays a crucial role in determining both the GSP resonance positions and the nanofocusing enhancement capability. The discrepancy between the observed GSP resonances and the simulation results is qualitatively explained as nonlocal effects occurring at the interfaces. The possibility of the convex groove array in realizing dual-band refractive index sensing in the VIS-NIR range was also experimentally demonstrated. A sensing performance with sensitivity up to 800 nm/RIU was obtained, as confirmed by our numerical simulations. We expect that our experimental results and theoretical analysis will be of help in improving our understanding of the GSP properties of convex groove structures, as well as for their practical applications in nanofocusing, light absorption, and surface-enhanced sensing of ultrasmall volumes.

ACKNOWLEDGMENTS

This work is supported by the National Natural Science Foundation of China (Grants No. 11974254, No. 61675139, and No. 11974253), the National Key R&D Program of China (Grant No. 2017YFA0303600), the Science Specialty Program of Sichuan University (Grant No. 2020SCUNL210), and the Innovation Program of Sichuan University (Grant No. 2018SCUH0074).

[1] W. L. Barnes, A. Dereux, and T. W. Ebbesen, Nature (London) **424**, 824 (2003).
[2] B. Prade, J. Y. Vinet, and A. Mysyrowicz, Phys. Rev. B **44**, 13556 (1991).
[3] M. Kuttge, W. Cai, F. J. Garcia de Abajo, and A. Polman, Phys. Rev. B **80**, 033409 (2009).
[4] H. Hu, Y. A. Akimov, H. Duan, X. Li, M. Liao, R. L. S. Tan, L. Wu, H. Chen, H. Fan, P. Bai, P. S. Lee, J. K. W. Yang, and Z. X. Shen, Nanoscale **5**, 12086 (2013).
[5] A. S. Roberts, T. Sondergaard, M. Chirumamilla, A. Pors, J. Beermann, K. Pedersen, and S. I. Bozhevolnyi, Phys. Rev. B **93**, 075413 (2016).
[6] D. K. Gramotnev and S. I. Bozhevolnyi, Nat. Photonics **8**, 14 (2014).
[7] S. I. Bozhevolnyi, Opt. Express **14**, 9467 (2006).
[8] S. I. Bozhevolnyi and J. Jung, Opt. Express **16**, 2676 (2008).
[9] T. Sondergaard, S. I. Bozhevolnyi, S. M. Novikov, J. Beermann, E. Devaux, and T. W. Ebbesen, Nano Lett. **10**, 3123 (2010).
[10] T. Sondergaard, S. M. Novikov, T. Holmgaard, R. L. Eriksen, J. Beermann, Z. Han, K. Pedersen, and S. I. Bozhevolnyi, Nat. Commun. **3**, 969 (2012).
[11] S. Raza, N. Stenger, A. Pors, T. Holmgaard, S. Kadkhodazadeh, J. B. Wagner, K. Pedersen, M. Wubs, S. I. Bozhevolnyi, and N. A. Mortensen, Nat. Commun. **5**, 4125 (2014).
[12] C. L. C. Smith, N. Stenger, A. Kristensen, N. A. Mortensen, and S. I. Bozhevolnyi, Nanoscale **7**, 9355 (2015).
[13] S. I. Bozhevolnyi, V. S. Volkov, E. Devaux, J. Y. Laluet, and T. W. Ebbesen, Nature (London) **440**, 508 (2006).
[14] T. Sondergaard and S. I. Bozhevolnyi, Phys. Rev. B **80**, 195407 (2009).
[15] T. Sondergaard, S. I. Bozhevolnyi, J. Beermann, S. M. Novikov, E. Devaux, and T. W. Ebbesen, Nano Lett. **10**, 291 (2010).
[16] J. Beermann, S. M. Novikov, T. Søndergaard, J. Rafaelsen, K. Pedersen, and S. I. Bozhevolnyi, J. Opt. Soc. Am. B **28**, 372 (2011).
[17] T. W. Ebbesen, H. J. Lezec, H. F. Ghaemi, T. Thio, and P. A. Wolff, Nature (London) **391**, 667 (1998).
[18] J. Beermann, T. Sondergaard, S. M. Novikov, S. I. Bozhevolnyi, E. Devaux, and T. W. Ebbesen, New J. Phys. **13**, 063029 (2011).
[19] D. K. Gramotnev, J. Appl. Phys. **98**, 104302 (2005).
[20] D. I. Yakubovsky, A. V. Arsenin, Y. V. Stebunov, D. Y. Fedyanin, and V. S. Volkov, Opt. Express **25**, 25574 (2017).
[21] Y. Cui, Y. He, Y. Jin, F. Ding, L. Yang, Y. Ye, S. Zhong, Y. Lin, and S. He, Laser Photonics Rev. **8**, 495 (2014).
[22] T. Sondergaard and S. I. Bozhevolnyi, New J. Phys. **15**, 013034 (2013).
[23] T. Søndergaard and S. I. Bozhevolnyi, Opt. Lett. **41**, 2903 (2016).
[24] Y. Yang, D. Zhu, W. Yan, A. Agarwal, M. J. Zheng, J. D. Joannopoulos, P. Lalanne, T. Christensen, K. K. Berggren, and M. Soljacic, Nature (London) **576**, 248 (2019).
[25] P. J. Feibelman, Prog. Surf. Sci. **12**, 287 (1982).
[26] P. Lalanne, W. Yan, K. Vynck, C. Sauvan, and J. P. Hugonin, Laser Photonics Rev. **12**, 1700113 (2018).
[27] W. Yan, R. Faggiani, and P. Lalanne, Phys. Rev. B **97**, 205422 (2018).
[28] E. J. H. Skjolstrup, T. Sondergaard, and T. G. Pedersen, Phys. Rev. B **97**, 115429 (2018).
[29] N. D. Lang and W. Kohn, Phys. Rev. B **1**, 4555 (1970).
[30] M. I. Stockman, Phys. Rev. Lett. **93**, 137404 (2004).